applied optics

Horizontally staggered lightguide solar concentrator with lateral displacement tracking for high concentration applications

HONGCAI MA[1,*] AND LIN WU[2,3]

[1]Changchun Institute of Optics, Fine Mechanics and Physics, Chinese Academy of Sciences, Changchun 130033, China
[2]Australian Centre for Visual Technologies, The University of Adelaide, SA 5005, Australia
[3]e-mail: lin.wu@adelaide.edu.au
*Corresponding author: hongcma@hotmail.com

Received 26 March 2015; revised 15 May 2015; accepted 10 June 2015; posted 10 June 2015 (Doc. ID 236984); published 3 July 2015

We present the design of a horizontally staggered lightguide solar concentrator with lateral displacement tracking for high concentration applications. This solar concentrator consists of an array of telecentric primary concentrators, a horizontally staggered lightguide layer, and a vertically tapered lightguide layer. The primary concentrator is realized by two plano-aspheric lenses with lateral movement and maintains a high *F*-number over an angle range of ±23.5°. The results of the simulations show that the solar concentrator achieves a high concentration ratio of 500× with ±0.5° of acceptance angle by a single-axis tracker and dual lateral translation stages.

OCIS codes: (080.2740) Geometric optical design; (350.6050) Solar energy; (220.4298) Nonimaging optics; (220.1770) Concentrators.

http://dx.doi.org/10.1364/AO.54.006217

1. INTRODUCTION

Solar energy is an attractive energy source with huge potential applications. Photovoltaic (PV) cells are generally identified as the most important components to realize photoelectricity power conversion. In order to save expensive semiconductor PV cell material, low-cost optical concentrators with a large area are utilized for concentrating sunlight onto a smaller area of high-efficiency PV cells. The optical concentrator can be either of the nonimaging or imaging type. The nonimaging concentrator, such as the compound parabolic concentrator (CPC), has a maximum theoretical concentration ratio by applying the edge-ray principle [1]. On the other hand, the imaging concentrators originate from the traditional imaging optical systems, such as the parabolic dish and trough concentrator [2]. Recently, planar lightguide solar concentrators [3–5] combined an imaging lens array with a lightguide layer with light injection facets have attracted much attention for their promising compactness, lightweight, and low-cost.

Season tracking of about ±23.5° can reduce the necessary acceptance angle of the solar concentrator, which is realized by a polar-aligned single axis tracker [6]. The external single axis tracker with daily modifications is suitable in the use for an equatorial mount and still has to rotate the whole CPV system along one axis to track seasonal changes. The planar lightguide solar concentrators can use tracking by lateral movement of the imaging lenses array with respect to the lightguide layer. Therefore, the lateral displacement tracking form avoids rotating the whole concentration photovoltaic (CPV) system and reduces the complexity of the Sun-tracking hardware. The optimized optical design for the planar lightguide solar concentrator through small lateral translations achieves a geometric concentration of 128× with 75% of the optical efficiency presented [7]. A planar, self-tracking solar concentrator system with an acceptance angle of over 40° is also demonstrated, which can achieve 150× effective concentration for a reasonably sized concentrator [8]. In the spectral splitting solar concentrator with double-lightguide layers, the capability of lateral displacement tracking has been explored for an aperture angle of ±24° [9]. A two-axis tracking scheme realized by a single-axis mechanical tracker and a translation stage is designed for <250× concentration with an 0.5° incidence angle, which has two-dimensional x–y tracking instead of horizontal movement in the x direction only [10]. However, the concentration ratios of the previous lightguide concentrators with lateral displacement tracking are not sufficient to make use of highly efficient PV cells. One feasible approach for high-concentration applications is that the primary concentrator in the lightguide concentrator takes the small focal spots and the small range of focused ray angles into account, further increasing the concentration ratio by a secondary concentrator. Therefore, this

paper proposes the utilization of two plano-aspheric lenses with lateral movement as the primary concentrator. This concentration approach has potential for an easily fabricated and highly integrated lightguide concentrator with high concentration.

In this paper, we investigate the design of a lightguide concentrator with lateral displacement tracking coupled with two plano-aspheric lenses with lateral movement. The horizontally staggered light injection facets are selected in the lightguide layer, which redirect the transverse sunlight in the lightguide layer without any leaking due to the injection points or directing surfaces downstream [11]. We also demonstrate the optical performance of the vertically tapered lightguide layer as a secondary concentrator to further increase the concentration of the horizontally staggered lightguide concentrator. The vertically tapered lightguide has the advantage of a straight and inclined edge with an easy structure. Especially in the lightguide layer with horizontal extension, the vertically tapered lightguide can achieve the same concentration performance while consuming few materials compared to the horizontally tapered lightguide.

2. METHOD OF CONCENTRATION WITH LATERAL DISPLACEMENT TRACKING

The proposed horizontally staggered lightguide solar concentrator with lateral displacement tracking consists of three parts: the primary concentrators array, horizontally staggered lightguide layer, and vertically tapered lightguide layer. In this concentration approach, the incoming sunlight is collected by an array of primary concentrators and coupled into the lightguide layer by the horizontally staggered light injection facets. The light injection facets redirect the sunlight by mirror reflection or total internal reflection (TIR). The horizontally staggered lightguide layer integrates the focused sunlight from the primary concentrators and allows the entire system to manage a unified output. Then the sunlight is directed into the tapered lightguide layer to further converge in a smaller exit area and finally toward a single PV cell, as shown in Fig. 1(a). With off-axis incident sunlight, the light injection facet can move laterally with the focal spot of the primary concentrator to track the Sun. Lateral displacement tracking is realized by lateral movement of the primary concentrators with respect to the lightguide layer, as shown in Fig. 1(b).

The concentration ratio of the primary concentrator is given as follows:

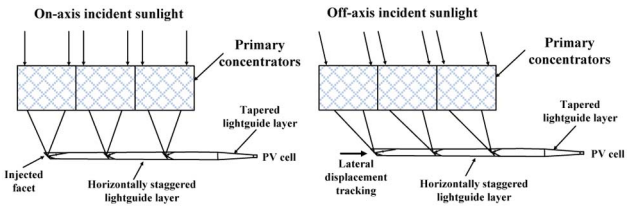

Fig. 1. Cross-sectional layouts of the horizontally staggered lightguide concentrator (a) with on-axis incident sunlight and (b) with off-axis incident sunlight with lateral displacement tracking.

$$C_{\text{primary}} = \frac{S_{\text{exit}}}{S_{\text{entrence}}}, \tag{1}$$

where S_{entrance} is the entrance area of the primary concentrator and S_{exit} is the focal spot area of the primary concentrator. The primary concentrator is preferred to keep small focal spots over a desired acceptance angle.

The numerical aperture (NA) of the primary concentrator defines the maximum focused ray angle and impacts the performance of the following tapered lightguide layer, which is introduced as

$$\text{NA} = n_1 \sin\theta = n_1 \sin\left[\arctan\left(\frac{1}{2(F/\#)}\right)\right], \tag{2}$$

where θ is the maximum focused ray angle of the primary concentrator, n_1 is the refractive index of the primary concentrator material, and $F/\#$ is the F-number of the primary concentrator.

Assuming a 45° reflective surface of the light injection facets, the ray with the maximum focused angle after reflection limits the concentration ratio of the tapered lightguide layer. The maximum theoretical concentration ratio of the tapered lightguide layer according to the etendue [1] is given as

$$(C_{\text{taper}})_{\max} = \frac{n_2}{n_1 \sin\theta}, \tag{3}$$

where n_2 is the refractive index of the tapered lightguide layer and horizontally staggered lightguide layer. Therefore, lowering the NA of the primary concentrator or increasing the $F/\#$ of the primary concentrator allows for a higher maximum concentration ratio of the tapered lightguide layer.

Finally, the total concentration ratio of the horizontally staggered lightguide concentrator is as follows:

$$C = C_{\text{primary}} \times C_{\text{taper}}. \tag{4}$$

3. ELEMENTS OF THE CONCENTRATOR

A. Primary Concentrator

The purpose of the primary concentrator is to focus the incident sunlight on the horizontally staggered light injection facet in the lightguide layer. In order to track seasonal changes, the primary concentrator has to achieve small focal spots over an angle range of ±23.5° and meet the angular extent of the Sun (±0.26°) and additional tracking tolerances. The two plano-aspheric lenses have been demonstrated to have good performances with low F-numbers over the desired angle range and be telecentric [12]. However, the increasing F-numbers of the two plano-aspheric lenses lead to a much smaller entrance pupil diameter than the second lens diameter, as shown in Fig. 2(a). This occurs because the imaging height of the two plano-aspheric lenses with high F-numbers is much larger than the entrance pupil diameter, where the diameter of the second lens equates approximately to the imaging height due to the telecentricity. The high physical area-to-pupil area ratio of the two plano-aspheric lenses with high F-numbers practically limits their utilization for concentration.

As shown in Fig. 2(a), the sunlight at every discrete angle covers only a small portion of the second lens aperture in the two plano-aspheric lens design. Inspired by the above feature,

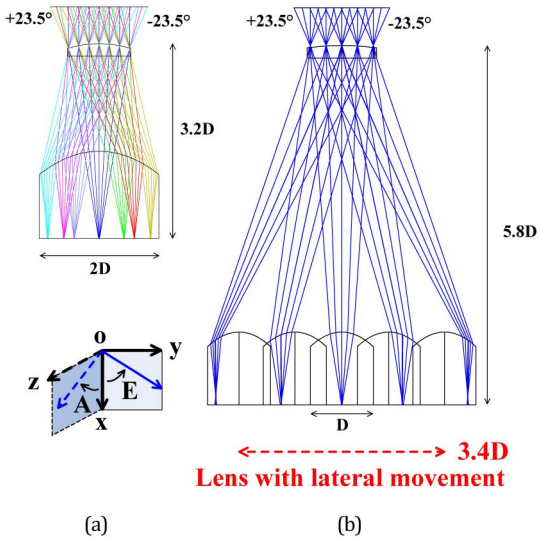

Fig. 2. Ray-trace diagrams at discrete incident angles over an angle range of ±23.5° for (a) two plano-aspheric lenses and (b) two plano-aspheric lenses with lateral movement. The diameters of the entrance pupil for both systems are equated and represented by D.

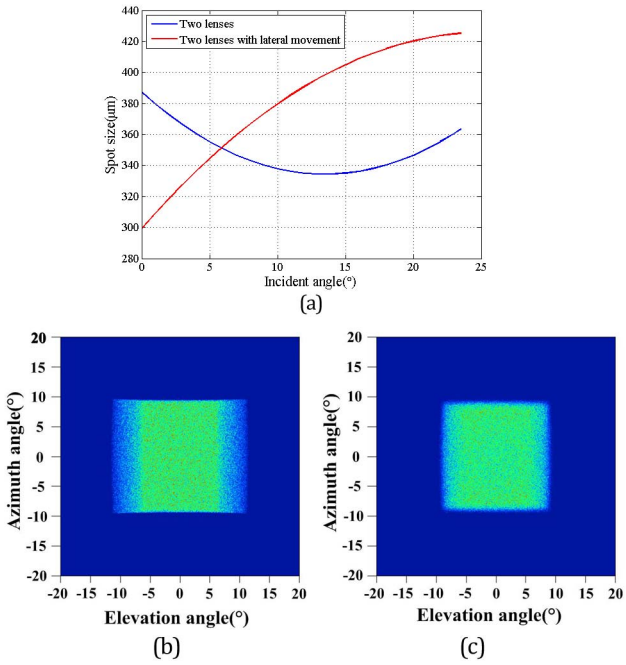

Fig. 3. (a) Focal spot sizes of the optimized two plano-aspheric lenses and two plano-aspheric lenses with lateral movement. The radiant intensity distributions of the light reaching the imaging plane over the angle range of ±23.5° for (b) two plano-aspheric lenses and (c) two plano-aspheric lenses with lateral movement. Elevation (E) and azimuth (A) angles are defined according the inset of Fig. 2(a).

the two plano-aspheric lenses with lateral movement are proposed to replace the previous two plano-aspheric lenses in this paper, as shown in Fig. 2(b). The diameter of the second lens would be less than the diameter of the first lens, such that it is possible to create an array of this two lens design. In the previous paper, the optical design of the two laterally moving plano–convex lenses has been proposed based on an extended simultaneous multiple surface algorithm and achieves a high concentration over the desired angular range [13]. Alternatively, in our design, the achievement of high concentration in the solar concentrator combines two lenses with high F-numbers with the tapered lightguide layer, and easily fabricated plano–convex lenses with spherical and parabolic surfaces are selected. The F-number of the two lenses with lateral movement is defined as the same value when the second lens is not decentered with respect to the first lens.

To meet the angular requirement with lateral displacement tracking, we optimize and evaluate two plano-aspheric lenses and two plano-aspheric lenses with lateral movement for small spot sizes over the angle range of ±23.5°, given weighted AM1.5 wavelengths from 0.4 to 1.8 μm [14] and at ±0.5° of uniform angular distributions. For the simulation of the solar concentrator, we have used the ZEMAX ray tracing software. Lenses select BK7 ($n = 1.516$) material and the first lenses have a 5 mm × 5 mm square aperture. For an easily fabricated structure, the aspheric surfaces of the first and second lenses are designed as spherical and parabolic surfaces, respectively. All optical systems are designed to meet the same F-number $f/2$, which also can be enhanced. The imaging plane of the lenses is set at the back surface of the second lens. The ray-trace diagrams of the optimized two plano-aspheric lenses and two plano-aspheric lenses with lateral movement are shown in Figs. 2(a) and 2(b), respectively.

Figure 3(a) shows a comparison of the focal spot sizes for two plano-aspheric lenses and two plano-aspheric lenses with lateral movement. Their focal spot sizes are comparative and slightly smaller than 430 μm. Figures 3(b) and 3(c) show the radiant intensity distributions of the light reaching the imaging plane for both systems. Their distributions of azimuth angles are similar, while the distribution of the elevation angles for the two plano-aspheric lenses with lateral movement due to its larger dimensions is slightly smaller than that of the two plano-aspheric lenses. The telecentricity of the two lens design constrains the range of the focused ray angles over the angle range of ±23.5° and is also necessary for high concentration of the tapered lightguide layer. It is an obvious advantage that the physical area-to-pupil area ratio of the two lenses with lateral movement is only 0.25 times that of the two plano-aspheric lenses.

B. Horizontally Staggered Lightguide Layer and Vertically Tapered Lightguide Layer

The horizontally staggered lightguide layer allows the entire system to manage a unified output, and the vertically tapered lightguide layer further decreases the exit area, as shown in Fig. 4(a). Due to the symmetrical radiant intensity distribution of the light reaching the imaging plane for the two lenses with lateral movement, the light injection facet in the horizontally staggered lightguide layer is suitable with a 45° reflective surface and we ensure the sunlight redirected in the lightguide layer by TIR without the use of reflective metallic coating. To compute the dimensions of the vertically tapered lightguide layer, the maximum number of TIRs for the extreme ray are needed [15] combined with the maximum focused ray angle of the

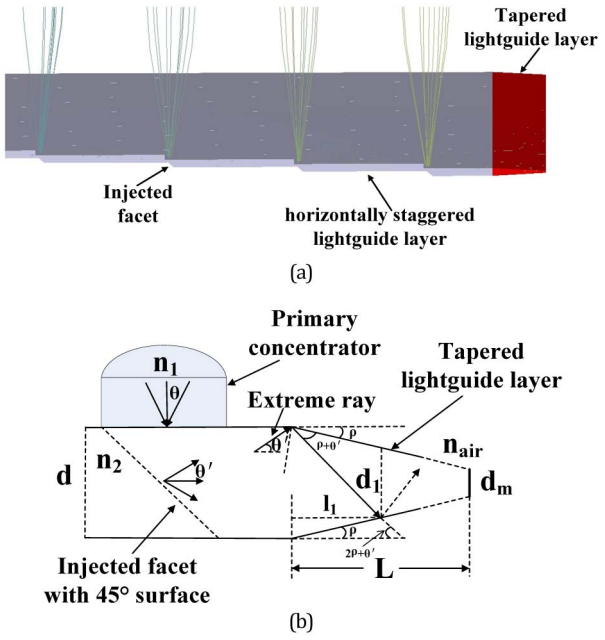

Fig. 4. (a) 3D layout of the horizontally staggered lightguide layer and the tapered lightguide layer. The primary concentrators are not shown. (b) Extreme ray-trace in the tapered lightguide layer and the definition of the relevant parameters to compute the dimensions of the tapered lightguide layer.

primary concentrator. The extreme ray-trace in the tapered lightguide layer and the definition of relevant parameters to compute the dimensions of the tapered lightguide layer are illustrated in Fig. 4(b).

When the focused sunlight transits across the boundary between the primary concentrator and the horizontally staggered lightguide layer, the maximum focused ray angle varies from θ to θ', which follows the law of refraction as

$$n_1 \sin\theta = n_2 \sin\theta'. \tag{5}$$

To ensure that the light injection facet in the horizontally staggered lightguide layer redirects the sunlight by TIR, the following relation must be satisfied:

$$\theta' < \theta_c - \pi/4, \tag{6}$$

where θ_c is the critical angle of the TIR on the surface of the light injection facet given by

$$\theta_c = \arcsin(1/n_2). \tag{7}$$

The theoretical mathematical relationship between the F-number of the primary concentrator and the refractive index of the lightguide layer is derived from Eqs. (2), (5)–(7) as

$$\frac{F}{\#} > \frac{1}{2\tan\left\{\arcsin\left[\frac{n_2}{n_1}\sin\left(\frac{\pi}{4} - \arcsin(n_2^{-1})\right)\right]\right\}}. \tag{8}$$

As shown in Fig. 5, the $F/\#$ ratios and refractive index material satisfying the requirement of TIR are in the upper right zone of the curve. The smaller $F/\#$ with large incident angle limited by TIR conditions at the light injection facet requires a higher refractive index of the lightguide layer. Using a lower refractive index material for the lightguide layer results in

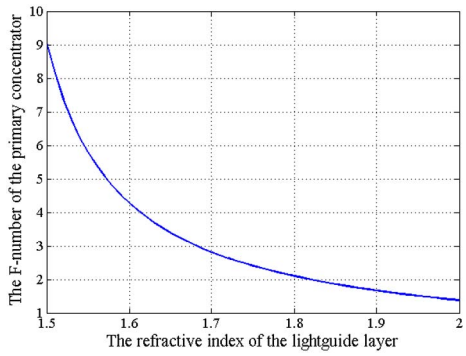

Fig. 5. Relationship between the F-number of the primary concentrator and the refractive index of lightguide layer.

a higher $F/\#$ of the primary concentrator, and this leads to a thicker structure of the two lenses. Therefore, the system optimal parameters are the result of a trade-off between the refractive index material of the lightguide layer and the $F/\#$ of the primary concentrator.

For the extreme ray, the length l_1 and the exit height d_1 of the tapered lightguide layer with the first TIR are derived by the following formula:

$$l_1 = d[\mathrm{tg}\rho + \mathrm{tg}(\theta' + 2\rho)]^{-1}, \tag{9}$$

$$d_1 = d - 2l_1\mathrm{tg}\rho, \tag{10}$$

where ρ is the tapered angle of the tapered lightguide layer and d is the entrance height of the tapered lightguide layer.

Following a similar procedure, the length l_m and the exit height d_m of the tapered lightguide with the mth TIRs are shown as follows:

$$l_m = d_{m-1}[\mathrm{tg}\rho + \mathrm{tg}(\theta' + 2m\rho)]^{-1} \tag{11}$$

$$d_m = d_{m-1} - 2l_m\mathrm{tg}\rho. \tag{12}$$

Furthermore, to ensure the sunlight transit in the tapered lightguide layer by TIRs, the following relation must also be satisfied:

$$\theta' \le \theta_c - (2m-1)\rho. \tag{13}$$

Finally, the concentration ratio of the tapered lightguide layer is defined as below:

$$C_{\mathrm{taper}} = d/d_m. \tag{14}$$

In this section, the concentration performance of the tapered lightguide layer is analyzed. The parameters of the tapered lightguide layer are designed for converging the ray from the optimized two lenses with lateral displacement in Section 3.A. As shown in Fig. 3(c), the maximum focused ray angle of the primary concentrator is about 10.3°. Therefore, we select a lightguide material with an index of refraction of 1.73 (based on the Schott SF10 datasheet) to satisfy Eq. (6). The refractive index $n_2 = 1.73$ of the lightguide layer increases the total concentration by 1.73× compared to the air output space and ensures that the light injection facet redirects the sunlight by TIR. Figure 6(a) shows the dependence of the

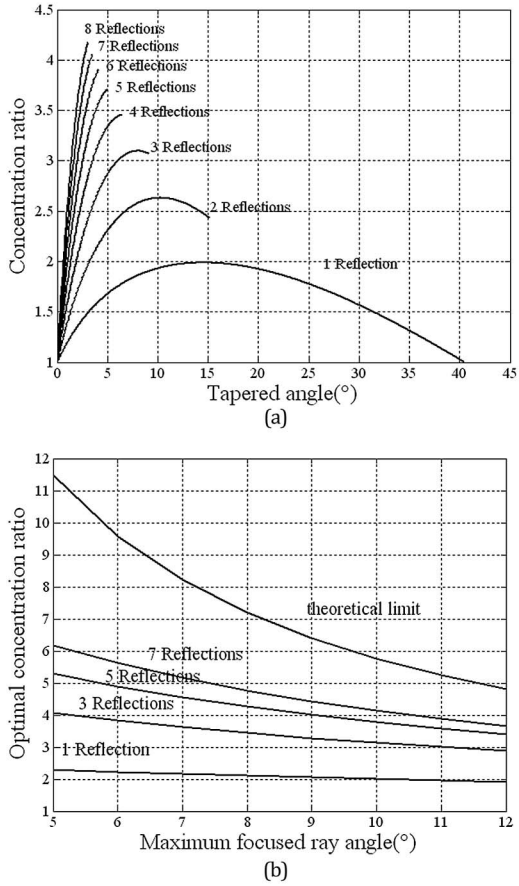

Fig. 6. (a) Dependence of the optimal concentration ratio on the tapered angle and the maximum number of TIRs assuming the maximum focused ray angle of 10.3°. (b) The optimal concentration ratio of the tapered lightguide layer varies with the maximum focused ray angle of the primary concentrator and the maximum number of TIRs.

optimal concentration ratio on the tapered angle and the maximum number of TIRs assuming the maximum focused ray angle of 10.3°. The optimal concentration ratio exists because a larger tapered angle implies that the exit height d_m of the tapered lightguide diminishes more rapidly. On the other hand, a larger tapered angle yields a larger reflection angle of the extreme ray. Therefore, the length L of the tapered lightguide is decreased, which increase the exit height d_m. Therefore, the observed optimal concentration ratio value is the result of a trade-off between these two effects, and it moves toward a smaller tapered angle as the number of TIRs increases. With the maximum number of TIRs such as 4, 5, 6, 7, 8, the optimal concentration ratios exist when the tapered angles are cut off by Eq. (13) and do not achieve the optimal concentration ratios of the tapered lightguide layer using mirror reflection.

Figure 6(b) shows that the optimal concentration ratio of the tapered lightguide layer varies with the maximum focused ray angle of the primary concentrator and the maximum number of TIRs. With the maximum focused ray angle decreasing, the optimal concentration ratio of the tapered lightguide increases. Therefore, the concentration ability of the tapered lightguide layer can benefit from the maximum focused ray angle of the primary concentrator with high F-number. With the

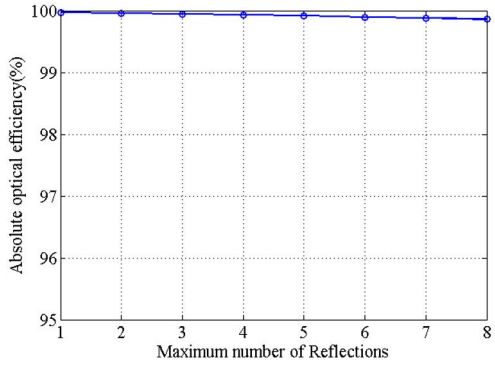

Fig. 7. Dependence of the optical efficiency on the maximum number of reflections when the optimal concentration ratios are achieved.

maximum number of TIRs increasing, the length of the tapered lightguide layer is enlarged, and its optimal concentration ratio increases but will lead to additional losses due to nonideal reflection. On the other hand, when the maximum focused ray angle of the primary concentrator increases, the optimal concentration ratio of the tapered lightguide layer diminishes but its concentration ability would approach to the theoretical limit value.

The dependence of the optical efficiency on the maximum number of reflections when the optimal concentration ratios are achieved has also been investigated, as shown in Fig. 7. When the maximum number of reflections the sunlight travels in the tapered lightguide layer increases, the optical transmission efficiency falls slightly while keeping high performance of more than 99.5%. The increase in the maximum number of reflections implies a larger length L of the tapered lightguide designed and the total distance that the sunlight rays travel in the tapered lightguide enlarges. As a result, the propagation loss due to the absorption of material increases in the tapered lightguide layer, while the absolute loss can be nearly neglected.

4. SIMULATIONS OF THE LIGHTGUIDE CONCENTRATOR WITH LATERAL DISPLACEMENT TRACKING

In the proposed tracking scheme, the lightguide concentrator follows the trajectory for each single day to track the daily Sun path by a polar axis tracker. Moreover, the lateral movement of the proposed optical design concurrently plays a role to track seasonal changes. The second lenses array and lightguide layer coupled with PV cells move independently, while the first lenses array are fixed. Therefore, dual individual lateral translation stages are necessary, which add to the tracking hardware complexity compared to the concepts where only the single lightguide layer moves relative to the primary lenses.

The goal of our design is a 500× concentration ratio with ±0.5° of the acceptance angle over the angle range of ±23.5°. We continue to use the design parameters of the two plano-aspheric lenses with lateral movement in Section 3.A and only adjust the focal plane of the lenses to the middle plane of the light injection facet. The detailed parameters of the optimized two lenses are listed in Table 1. The two lens array is arranged with a total amount of 20 in elevation in the lightguide

Table 1. Detailed Parameters of the Two Plano-Aspheric Lenses with Lateral Movement

Parameters	Lens 1	Lens 2
Aperture (mm)	5 × 5	5 × 5
Radius (mm)	19.2	2.6
Conic	0	−1
Thickness (mm)	1	5.4
Distance between lenses (mm)	22.85	

concentrator. The lens array has MgF_2 AR coatings of 150 nm on the front and back surfaces of the first lenses and the front surface of the second lenses. SF10 of the lightguide layer material with a refractive index of 1.73 is selected. The light injection facet of the lightguide layer has a size of 0.45 mm × 0.45 mm. The symmetric point of the light injection facet is located at the geometric center of the focal spot with lateral displacement tracking. The resulting concentration ratio of the primary concentrator is $C_{primary} = 123.5\times$, and this makes the required concentration ratio of the tapered lightguide layer $C_{taper} = 4.05\times$. From Fig. 6(a), we obtain 3.5° of the responding tapered angle of the tapered lightguide layer with seven TIRs. As a design result, Fig. 8 shows the example of the optimized lightguide concentrator with 10° of the sunlight incident angle.

Figure 9 shows the dependences of transmission efficiency and efficiency of Fresnel losses on incident angle. The transmission efficiency is over 88% and maintains a good average value of 90.7% over the angle range of ±23.5°. The average efficiency of Fresnel losses is 6.6% over the angle range of ±23.5°. The reflection losses of the front and back surfaces of the first lens are both 2% and increase slightly with increasing angles of incident sunlight. However, the reflection loss of the front surface of the second lens increases dramatically from 1.9% to 5.3% with the incident angle varying from 0° to ±23.5°. The reason is that the deviation angles of the chief rays in this surface enlarge rapidly due to the telecentricity.

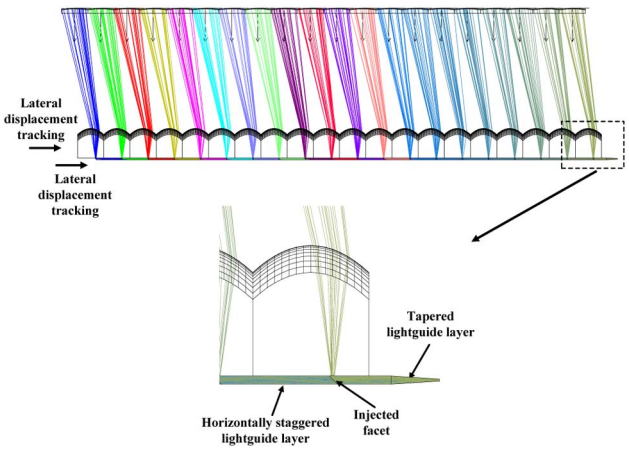

Fig. 8. Example of the optimized lightguide concentrator with the 10° sunlight incident angle. The fixed first lenses and the second lenses with lateral movement play a role in the telecentric primary concentrator. The lightguide layer combined with a PV cell move laterally for tracking the focal spots of the above primary concentrators.

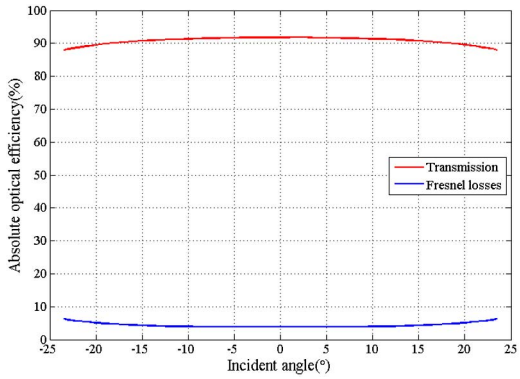

Fig. 9. Dependencies of transmission efficiency and efficiency of Fresnel losses on incident angle. The efficiency of Fresnel losses here includes the front and back surfaces of the first lens and the front surface of the second lens.

These efficiencies can be further improved by the use of the AR coating with a multilayer structure. The reflection loss that occurs between the second lens and the lightguide layer is 0.38% because the refractive index change is large at the boundary. The lens array has an absorption of 0.14%, and the lightguide including absorption and nonideal reflection has total losses of 2.08% on average. Additionally, the small lateral displacements of the second lenses and the lightguide layer with respect to the second lenses are only ±8.7 and ±1.8 mm, respectively.

5. CONCLUSIONS

The proposed horizontally staggered lightguide concentrator with lateral displacement tracking achieves a high concentration ratio of 500× and a good average transmission efficiency of 90.7% over the angle range of ±23.5°, which is accomplished by a single-axis tracker and dual translation stages. The two plano-aspheric lenses with lateral movement with high *F*-numbers are necessary for high concentrations of the tapered lightguide layer in the lightguide concentrator. The material of the vertically tapered waveguide layer preferably possesses a higher refractive index than the lenses for effective performances. This lightguide concentrator with lateral displacement tracking is an easily fabricated structure, with high integration of PV cells connection and a uniform flux radiation received. The telecentric primary concentrator in this paper is also compatible with the planar waveguide solar concentrator.

REFERENCES

1. R. Winston, J. C. Miñano, and P. Benitez, *Nonimaging Optics*, N. Shatz and J. C. Bortz, eds. (Elsevier Academic, 2005), pp. 1–68.
2. A. Luque and S. Hegedus, eds., *Handbook of Photovoltaic Science and Engineering*, 2nd ed. (Wiley, 2003) pp. 449–504.
3. J. H. Karp, E. J. Tremblay, and J. E. Ford, "Planar micro-optic solar concentrator," Opt. Express **18**, 1122–1133 (2010).
4. B. L. Unger, G. R. Schmidt, and D. T. Moore, "Dimpled planar lightguide solar concentrators," in *Proceedings of International Optical Design Conference* (Optical Society of America, 2010), paper ITuE5P.
5. D. Moore, G. Schmidt, and B. Unger, "Concentrated photovoltaic stepped planar light guide," in *International Optical Design Conference*, OSA Technical Digest (CD) (Optical Society of America, 2010), paper JMB46P.

6. A. Rabl, *Active Solar Collectors and Their Applications* (Oxford University, 1985).
7. J. M. Hallas, K. A. Baker, J. H. Karp, E. J. Tremblay, and J. E. Ford, "Two-axis solar tracking accomplished through small lateral translations," Appl. Opt. **51**, 6117–6124 (2012).
8. V. Zagolla, E. Tremblay, and C. Moser, "Proof of principle demonstration of a self-tracking concentrator," Opt. Express **22**, A498–A510 (2014).
9. H. Ma, Q. Meng, S. Xu, J. Dong, and W. Li, "High-integrated spectral splitting solar concentrator with double-light guide layers," Opt. Eng. **53**, 105102 (2014).
10. Y. Liu, R. Huang, and C. K. Madsen, "Two-axis tracking using translation stages for a lens-to-channel waveguide solar concentrator," Opt. Express **22**, A1567–A1575 (2014).
11. O. Selimoglu and R. Turan, "Exploration of horizontally staggered light guides for high concentration CPV applications," Opt. Express **20**, 19137–19147 (2012).
12. E. Tremblay, V. Zagolla, D. Loterie, and C. Moser, "Self-tracking planar concentrator using a solar actuated phase-change mechanism," Proc. SPIE **8620**, 862011 (2013).
13. F. Duerr, Y. Meuret, and H. Thienpont, "Tracking integration in concentrating photovoltaics using laterally moving optics," Opt. Express **19**, A207–A218 (2011).
14. NREL, "AM1.5G solar spectrum irradiance data," http://rredc.nrel.gov/solar/spectra/am1.5/.
15. A. Goetzberger and O. Schirmer, "Second stage concentration with tapers for fluorescent solar collectors," Appl. Phys. **19**, 53–58 (1979).